UNCERTAINTY PROPAGATION FROM ATMOSPHERIC PARAMETERS TO SPARSE HYPERSPECTRAL UNMIXING

Marian-Daniel Iordache[1], *Nitin Bhatia*[1], *José M. Bioucas-Dias*[2], *Antonio Plaza*[3]

[1] Flemish Institute for Technological Research (VITO), Boeretang 200, BE-2400 Mol, Belgium
[2]Instituto de Telecomunicações and Instituto Superior Técnico,
Universidade de Lisboa, 1049-001, Lisbon, Portugal
[3]Hyperspectral Computing Laboratory, Department of Technology of Computers and Communications,
University of Extremadura, E-10071 Cáceres, Spain

ABSTRACT

Sparse hyperspectral unmixing is a widely used technique in remote sensing data characterization. It aims at inferring, from a large spectral library, the pure spectral signatures (endmembers) present in each pixel of a hyperspectral image, jointly with their corresponding abundances. The input to sparse unmixing is represented, thus, by a hyperspectral image acquired from a platform flying at high altitude and a spectral library compiled using laboratory measurements. The reflectance datacube results from a complex ensemble of algorithms which translate the digital numbers stored by the sensor to meaningful ground reflectance, including the removal of atmospheric influence. A recurrent question in the research community does not have an answer yet: how does the atmospheric composition at the time of the flight influence the fractional abundances retrieved *via* sparse unmixing? This is a fundamental question, as the atmospheric parameters are subject to uncertainties, being very difficult to know them in all pixels. In this paper, we investigate how the uncertainty in two atmospheric parameters: water vapor content and visibility range, propagates to the final abundance maps via atmospheric correction of the sensed image. Our experiments reveal that sparse unmixing is more robust to uncertainty in those parameters and performs better in terms of accuracy than unmixing with image-based endmembers.

Index Terms— Sparse unmixing, atmospheric correction, uncertainty, spectral libraries

1. INTRODUCTION

Hyperspectral unmixing (see [1] and the references therein) is a concept which defines the processing steps applied to a hyperspectral image in order to derive the pure materials present in the image (endmembers), their spectral signatures and their respective fractional abundance (the relative areas occupied by the endmembers in each pixel of the image). In a classical spectral unmixing setup, a few typical operations are performed: data dimensionality reduction (optional), endmember inference and inversion (estimation of abundances). The estimation of endmembers, which can be done by extracting pure pixels from the image itself (*e.g.*, NFINDR [2], Pixdel Purity Index – PPI [3]) or by generating virtual endmembers based on the spatial distribution of the data in a multi-dimensional space (*e.g.*, Vertex Component Analysis – VCA [4], Minimum Volume Simplex Analysis – MVSA [5]), constitutes a critical step in highly mixed scenes, where pure pixels can not be found for all the endmembers or the geometric representations of the data result in non-realistic endmembers (*e.g.*, negative ones).

Recent research [6] highlights sparse unmixing as a powerful alternative to classical methods employing endmember extraction/generation. Sparse unmixing represents a class of spectral unmixing methods which rely on the use of available spectral libraries (collections of pure spectra, measured by a spectrometer in a controlled environment, *e.g.* laboratory). The unmixing is formulated as a convex optimization problem aiming at selecting, in each pixel, a subset of library members which accurately explains the observed spectrum. As the spectral libraries contain a large number of spectra compared to the number of endmembers in one pixel, the sparsity of the vector of fractional abundances arises as a natural condition. Thus, the sparse unmixing can be expressed as a convex optimization problem in which the ideal trade-off between the accurate reconstruction of the data and the sparsity of the vector of abundances is searched for.

Several factors are proven to strongly influence the accuracy of sparse unmixing. Among these factors, the mutual coherence of the spectral libraries (cite) and the level of noise contaminating the data are two of the most investigated ones [7, 8]. However, a recurrent question in this research area does not have an answer yet: what is the impact of the different measuring conditions of the data and library in the final abundance maps?

The main difference in the measuring conditions is represented by the presence of atmospheric effects in the image which obviously do not affect the library spectra. The spectral libraries are compiled from measurements made with spectrometers, on the ground, in open air or in a laboratory. However, the spectrum of one specific pixel, captured by the sensor flying at high altitude, is contaminated with contributions from neighboring pixels and, most important, atmospheric effects.

Schematically, the typical processing of the raw data downloaded from the sensor includes: 1) spectral and radiometric calibration (which results in the so-called at-sensor radiance) and 2) atmospheric correction (AC), intended to remove the atmospheric artifacts from the observed spectra while transformimg the at-sensor radiance to ground radiance or reflectance. The ground reflectance (or radiance) obtained after AC is then input to unmixing.

From the two aforementioned processing steps, we consider in this study the atmospheric correction only. The spectral and radiometric calibration of the data is a procedure which can benefit from accurate definition of the calibration coefficients (*e.g.*, by performing laboratory measurements and in-flight simulations on a regular basis). However, the atmospheric correction is a complex ensemble

of algorithms which require accurate knowledge of the atmospheric parameters (in the case considered in this study, visibility range and water vapor content) in all pixels. We note that this information is not available in practice, as it is infeasible to measure these parameters for each pixel. In practice, two approaches can be taken to tackle such lack of information: 1) measurements from ground stations or from ground equipments in (or close to) the sensed area are set as input values for atmospheric correction in all pixels, or 2) image-based methods are implemented to estimate the parameters on a per-pixel basis. On the one hand, the values of the atmospheric parameters are very likely to vary across the pixels, due to the fact that the atmosphere is a dynamic system (variable in time and space). On the other hand, the image-based methods are prone to inherent modeling errors. It results that the atmospheric correction rarely benefits from exact values of the parameters, which makes impossible the removal of all atmospheric artifacts from the data. The uncertainty affecting the atmospheric correction parameters is thus propagated to the subsequent applications. Moreover, the spectral libraries employed in sparse unmixing are ideally free from these artifacts, which leads to an intrinsic mismatching, not present in the classical unmixing using extracted endmembers. In this paper, we analyze how the uncertainty in the atmospheric parameters are propagated to sparse unmixing results represented by the fractional abundances. To our knowledge, there is no similar study available in the literature.

The paper is structured as follows. Section 2 shortly reviews sparse unmixing and atmospheric correction from a theoretical point of view. Section 3 presents the methodology employed to track the uncertainty propagation. Section 4 presents experimental results in a simulated environment. Section 5 concludes the paper with observations and hints to future work.

2. THEORETICAL BACKGROUND

In this section, we shortly review the theoretical concepts related to sparse unmixing and atmospheric correction.

2.1. Atmospheric Correction

The term Atmospheric Correction (AC) denotes the ensemble of algorithms applied to a (spectrally and radiometrically) calibrated image, delivered by a sensor, intended to derive a ground radiance/reflectance datacube which is free of atmospheric effects. The at-sensor sensed spectrum of a pixel contains data from the actual target contaminated with spectral artifacts introduced by neighboring pixels (the so-called adjacency effect) and with atmospheric effects due to light scattering depending on the composition of the atmosphere at the time of the flight. In this work, we neglect the adjacency effect, as the influence of spatial neighborhoods is given by a variety of factors (target albedo, topography, flight direction, solar position) which are difficult to simulate. Among the AC parameters, the water vapor concentration $[g \cdot cm^{-2}]$ and the aerosol optical thickness (related to atmospheric visibility $[km]$) are the ones with highest impact on the spectral quality of the data.

The content of WV in the atmosphere introduces features at well-established wavelengths (resulting in the so-called water absorption features), while the visibility affects the amplitude of the spectrum in different spectral regions. The AC requires accurate knowledge of these parameters in each pixel of the image, which is unfeasible in practice. Over- and under- estimation of WV results in peaks and dips at the water vapor absorption bands, respectively [9]. The influence of VIS on the retrieved spectrum is nonlinear and varies with the target albedo: for low albedo (approximately 0.3 for MODerate resolution atmospheric TRANsmission 4 – MODTRAN-4 [10] software), the increase or decrease in VIS results in increased or decreased amplitude of the spectrum, respectively. For high albedo, the effect is reverted. After AC, potential miscalibrations of the at-sensor radiance data lead to noisy reflectance values at the affected bands. Usually, smoothing is applied to the reflectance spectra as a final processing step before sending the data to an user. It results that the noise affecting remotely sensed hyperspectral data, no matter the reasons which generate it (dark current, miscalibration, among others) is most of the times band-correlated.

2.2. Sparse Unmixing

We consider that the data follows the linear mixing model, in which each spectrum in the data can be expressed as a linear combination of the spectra of the endmembers. Under this assumption and given a spectral library $\mathbf{A}$, the observed spectrum $\mathbf{y}$ for one pixel can be expressed as

$$\mathbf{y} = \mathbf{A}\mathbf{x} + \mathbf{n}, \tag{1}$$

where $\mathbf{x}$ is the vector of fractional abundances and $\mathbf{n}$ is a vector collecting the errors that affect the measurement process (*e.g.,* noise). The fractional abundances are subject to the so-called *non-negativity constraint* (ANC) and *the sum-to-one constraint* (ASC) (the abundances cannot be negative and they should sum to one) [1].

In a sparse unmixing approach, the solution of the unmixing is the sparsest combination of library members which explains with high accuracy the explained data. A typical formulation of a sparse regression optimization to perform hyperspectral unmixing is expressed as

$$\begin{aligned} \min_{\mathbf{x}} \quad & \|\mathbf{y} - \mathbf{A}\mathbf{x}\|_2^2 + \lambda \|\mathbf{x}\|_1 \\ \text{subject to:} \quad & \mathbf{x} \geq 0, \end{aligned} \tag{2}$$

where the first term is the data-fitting term and the second term is the ℓ_1-norm of $\mathbf{x}$ which imposes the sparsity, while λ is a regularization parameter which weights the two terms of the objective function.

3. EXPERIMENTAL SETUP AND METHODOLOGY

A simulated image of 100×100 pixels containing 9 endmembers randomly selected from a library $\mathbf{A} \in \mathbb{R}^{224 \times 240}$ (a subset of 240 spectra from the USGS library available online[1]) is used in our experiments. The library spectra are assigned to 55 groups, each group representing one distinct material. In order to simulate spectral endmember variability in the scene, two of the nine endmembers are chosen from the same group (chlorite). The scene is generated following the methodology presented in [7] (see the procedure to generate second simulated image, DC2, in this paper). The fractional abundances display spatial smoothness and are generated according to the LMM in which the ANC and ASC are enforced. This image serves as a ground-truth reflectance image, for which the abundances of all endmembers are known in each pixel.

The ground-truth reflectance image is then upscaled to at-sensor radiance using the MODTRAN software. We assume the data is acquired by the HyMap[2] sensor in 126 spectral bands. The ground-truth reflectance spectra are thus resampled to the HyMap wavelengths. To simulate the actual flight, the viewing and illumination geometry (sensor configuration) are set using real data from a

[1] See http://speclab.cr.usgs.gov/spectral-lib.html

[2] See http://www.dlr.de/eoc/en/desktopdefault.aspx/tabid-6206/10515_read-35586/

previous flight, available at VITO. The two atmospheric parameters considered in our study are set to $wv = 1.5\text{g} \cdot \text{cm}^{-2}$ for WV and $vis = 30\ km$ for VIS, in order to establish the true atmospheric conditions at the time of the flight. These parameters are equal for all pixels. The simulated at-sensor radiance image represents the (radiometrically and spectrally) calibrated image used as input to atmospheric correction.

The at-sensor radiance is transformed to ground reflectance using the Central Data Processing Center (CDPC) [11], which is the standard processing chain at the Flemish Institute for Technological Research (VITO–TAP), Mol, Belgium. The CDPC has tradition of several years in the processing of remotely sensed data and uses MODTRAN in the AC process. To simulate uncertainty in the AC parameters, we consider that the WV varies between 1.2 and 1.8 $g \cdot cm^{-2}$ with an increasing step of 0.02 $g \cdot cm^{-2}$, while VIS varies between 20 and 40 km with an increasing step of 2 km. The combinations of all the considered values result in 340 processing cases. The 340 reflectance images are subsequently contaminated with spectrally correlated noise obtained from low-pass filtering i.i.d. Gaussian noise, using a normalized cut-off frequency of $5\pi/L$, where L is the number of bands, and having the signal-to-noise ratio (SNR $\equiv \mathbb{E}\left\|\mathbf{Ax}\right\|^2 / \mathbb{E}\left\|\mathbf{n}\right\|_2^2$) fixed to 30dB.

Unmixing is performed for all generated reflectance images using both extracted endmembers inferred *via* VCA and the spectral library $\mathbf{A}$. When VCA is employed, we assume that the number of endmembers is known and equal to the true one (nine). The sparse unmixing algorithm employed to solve the optimization problem (2) is the Sparse Unmixing via variable Splitting and Augmented Lagrangian (SUnSAL) [12] algorithm. In each processing case, the parameter λ takes the following values: 0, 0.01, 0.03, 0.05, 0.1, 0.2 and 0.3. For each image, the unmixing is repeated three times (the contamination with noise being simulated separately each time) and only the average of best performances (among all considered values of λ) are reported. We expect that the sparsity constraint has limited or no impact on the data employing extracted endmembers.

The performance discriminator is the signal to reconstruction error [6]: SRE $\equiv \mathbb{E}[\|\mathbf{x}\|_2^2]/\mathbb{E}[\|\mathbf{x} - \hat{\mathbf{x}}\|_2^2]$, measured in dB: SRE(dB) $\equiv 10\log_{10}(\text{SRE})$, where $\mathbf{x}$ is the true quantity and $\hat{\mathbf{x}}$ is the estimated one. We use this indicator for both reflectance and unmixing. Higher SRE(dB) indicates better performance (in unmixing) or better spectral quality (in reflectance). The unmixing performance is reported both at individual member (each library member is considered to represent one material) and at group level (the abundances of the members belonging to one group are added together to define the abundance of the material assigned to the group).

4. EXPERIMENTAL RESULTS

First, we analyze the influence of AC parameters on the spectral quality. Fig. 1 shows the evolution of the SRE(dB), computed for reflectance, w.r.t. the AC parameters, for both noiseless and noisy data..

Fig. 1.a), which refers to noiseless reflectance, proves the importance of correctly setting the parameters during the AC. A peak performance is visible when the two considered parameters are set to the true values. It can be observed that the spectral quality degrades when inaccurate values are employed. The WV impact is stronger than the VIS influence. The same Figure suggests that an overestimation of VIS is preferrable to underestimation in the considered setup. From Fig. 1.b), which corresponds to the data affected by noise, it is obvious that the advantage of correctly setting the AC

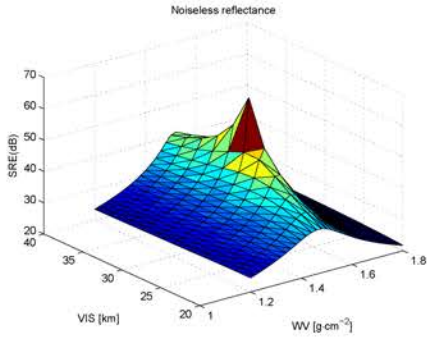

(a) Noiseless data

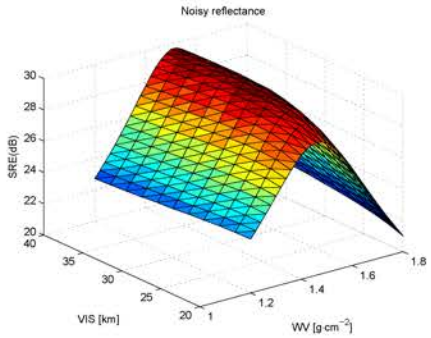

(b) Noisy data

Fig. 1. Spectral quality measured by SRE(dB) for (a) noiseless data and (b) noisy data.

parameters is strongly attenuated from the point of view of spectral quality. No performance peak is visible in this figure. However, the WV is still a determinant factor in the data quality and it is confirmed that the VIS values have a weaker (although still visible) impact on the data quality.

The noiseless data is, however, an ideal case which is not encountered in practice. For this reason, we center our analysis related to unmixing on the noisy data. In Fig. 2, we plot the SRE(dB) computed for the unmixing when both the image-based endmembers and the library are used. Fig. 2.a) shows the performance computed for individual endmembers, while Fig. 2.b) displays the performance computed for groups (materials).

Fig. 2 displays different trends of the unmixing performance when the two approaches are used. On the one hand, the unmixing with image-based endmembers shows highly unstable, irregular performance and there is no visible advantage of knowing the correct AC parameters. On the other hand, sparse unmixing employing the spectral library has a smooth performance variation and takes advantage of the corect setting of the AC parameters (see the higher performance around the correct WV value). Although none of the two methods reaches excellent perfromance when the performance is computed for individual endmembers, it is worth noting that spectral unmixing employing the spectral library is slightly more performant than the unmixing with image-based endmembers when the AC parameters are set to values close to the true ones, while a smooth performance degradation is visible in the other cases. Another observation is that the unmixing with spectral library is robust to the VIS variation in the considered setup (note that the unmixing per-

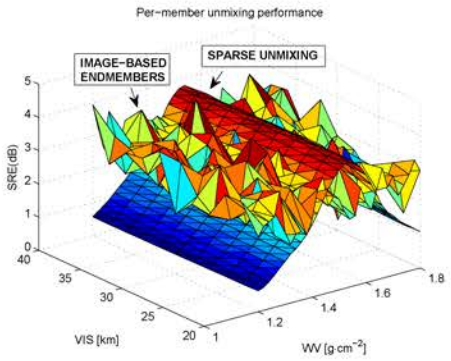

(a) Per-member performance

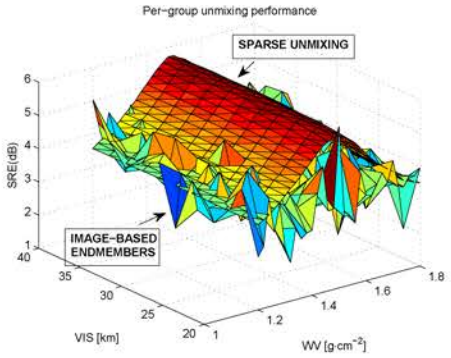

(b) Per-group performance

Fig. 2. Spectral unmixing quality measured by SRE(dB) for (a) individual endmembers and (b) groups of endmembers (materials).

formance is approximately constant when VIS varies, although the spectral quality decreases for underestimated VIS - see Fig. 1.b). The performances plotted in Fig. 2 highlight more clearly the advantages of sparse unmixing over the unmixing employing image-based endmembers. It is worth noting that the unmixing performances computed for groups of materials are superior to the performances with individual endmembers in all processing cases, regardless of the taken approach. In addition, the sparse unmixing is most of the times superior, which indicates that, as a consequence of noise, the identification of the exact library member contributing to the data is difficult (as seen from Fig. 2.a), but the correct material is better identified as compared to the image-based method. This is a remarkable finding, as the generated data favors the unmixing with image-based endmembers due to the presence of pure pixels for all endmembers. It is expected that the unmixing using image-based endmembers loses accuracy when the pure pixel assumption is not met. Moreover, the performance trend in Fig. 2.b) suggest that the unmixing with image-based endmembers might perform better than the unmixing with spectral library if the errors in the estimated WV are larger than 0.2 $g \cdot cm^{-2}$, approximately. However, from our practical experience in using the CDPC, such an error in WV values is usually not tolerated, as it results in visible peaks or dips at the water absorption bands. The presented results are also in line with the findings in our previous work [9], where it is shown that unmixing with library signatures is superior to unmixing with image-based endmembers when the true set of endmembers is known.

5. CONCLUSIONS AND FUTURE WORK

In this work, the propagation of uncertainty from atmospheric correction parameters to sparse hyperspectral unmixing was investigated. Our experiments with simulated data were designed to tackle one of the hot topics in our research community: how important is the difference in acquisition conditions between a library and a reflectance image when it comes to unmixing? It was shown that sparse unmixing is a robust application in the sense that it achieves higher performance than unmixing employing image-based endmembers, when the data is atmospherically corrected using parameters which do not deviate significanlty from the true values. The performances of sparse unmixing vary smoothly with the atmospheric parameters variation, which is not the case when the image-based approach is followed. This study opens a plethora of possibilities for future research. Other processing parameters can be included in the experiments, such as the adjacency window related to the background contribution to one pixel. Other sparse unmixing algorithms can be tested, including dictionary pruning. Other applications (*e.g.*, image classification, target detection, image segmentation) can be also explored following a similar approach. The reproduction of this study in a real scenario also represents a challenge, due to the lack of images benefiting from knowledge of the true values of the atmospheric parameters in all pixels.

6. REFERENCES

[1] J. M. Bioucas-Dias, A. Plaza, N. Dobigeon, M. Parente, Q. Du, P. Gader, and J. Chanussot, "Hyperspectral unmixing overview: Geometrical, statistical and sparse regression-based approaches," *IEEE Journal of Selected Topics in Applied Earth Observations and Remote Sensing*, vol. 5, no. 2, pp. 354–379, 2012.

[2] M. Winter, "N-FINDR: An algorithm for fast autonomous spectral endmember determination in hyperspectral data," *Proceedings of SPIE*, vol. 3753, pp. 266–277, 1999.

[3] J. W. Boardman, "Automating spectral unmixing of aviris data using convex geometry concepts," *Proc. Ann. JPL Airborne Geosci. Workshop*, vol. 1, pp. 11–14, 1993.

[4] J. Nascimento and J. Bioucas-Dias, "Vertex component analysis: a fast algorithm to unmix hyperspectral data," *IEEE Transactions on Geoscience and Remote Sensing*, vol. 43, no. 4, pp. 898–910, 2005.

[5] Jun Li, A. Agathos, D. Zaharie, J.M. Bioucas-Dias, A. Plaza, and Xia Li, "Minimum volume simplex analysis: A fast algorithm for linear hyperspectral unmixing," *Geoscience and Remote Sensing, IEEE Transactions on*, vol. 53, no. 9, pp. 5067–5082, Sept 2015.

[6] D. Iordache, J. Bioucas-Dias, and A. Plaza, "Sparse unmixing of hyperspectral data," *IEEE Transactions on Geoscience and Remote Sensing*, vol. 49, no. 6, pp. 2014–2039, 2011.

[7] D. Iordache, J. M. Bioucas-Dias, and A. Plaza, "Total variation spatial regularization for sparse hyperspectral unmixing," *IEEE Transactions on Geoscience and Remote Sensing*, vol. 50, no. 11, pp. 4484–4502, 2012.

[8] M.-D. Iordache, J.M. Bioucas-Dias, A. Plaza, and B. Somers, "Music-csr: Hyperspectral unmixing via multiple signal classification and collaborative sparse regression," *Geoscience and Remote Sensing, IEEE Transactions on*, vol. 52, no. 7, pp. 4364–4382, July 2014.

[9] N. Bhatia, M.-D. Iordache, A. Stein, I. Reusen, and V. Tolpekin, "Propagation of uncertainty in atmospheric parameters to hyperspectral unmixing," *IEEE Journal of Selected Topics in Applied Earth Observations and Remote Sensing (submitted)*, 2016.

[10] A. Berk, G.P. Anderson, P.K. Acharya, J.H. Chetwynd, L.S. Bernstein, E.P. Shettle, M.W. Matthew, and S.M. Adler-Golden, "Modtran 4 users manual," *Technical Report*, 1999.

[11] J. Biesemans, S. Sterckx, E. Knaeps, K. Vreys, S. Adriaensen, J. Hooy-Berghs, K. Meuleman, P. Kempeneers, B. Deronde, J. Everaerts, D. Schlapfer, and J. Nieke, "Image processing workflows for airborne remote sensing," *Proc. 5th EARSeL Workshop on Imaging Spectroscopy, Bruges, Belgium*, pp. 1–14, April 23–25 2011.

[12] J. Bioucas-Dias and M. Figueiredo, "Alternating direction algorithms for constrained sparse regression: application to hyperspectral unmixing," *2nd Workshop on Hyperspectral Image and Signal Processing: Evolution in Remote Sensing*, vol. 1, pp. 1–4, Reykjavik, Iceland, 2010.